

SELECTED TOPICS IN APPLIED PHYSICS

Evolution of corundum-structured III-oxide semiconductors: Growth, properties, and devices

To cite this article: Shizuo Fujita *et al* 2016 *Jpn. J. Appl. Phys.* **55** 1202A3

View the [article online](#) for updates and enhancements.

You may also like

- [Effect Infestation by *Sesamia cretica* L. Insect in some Characteristics of Growth for Varieties of Yellow Corn](#)
Mohammed Rakan Shallal, Abdul Jabar K. Ibrahim and Arqam Alomari
- [Application of halide vapor phase epitaxy for the growth of ultra-wide band gap \$\text{Ga}_2\text{O}_3\$](#)
Xiangqian Xiu, Liying Zhang, Yuewen Li et al.
- [Development of stable Grid service at the next generation system of KEKCC](#)
T. Nakamura, G. Iwai, H. Matsunaga et al.



Evolution of corundum-structured III-oxide semiconductors: Growth, properties, and devices

Shizuo Fujita^{1*}, Masaya Oda^{2*}, Kentaro Kaneko¹, and Toshimi Hitora²

¹Photonics and Electronics Science and Engineering Center, Kyoto University, Kyoto 615-8520, Japan

²FLOSFIA Inc., Kyodai-Katsura Venture Plaza, Kyoto 615-8245, Japan

*E-mail: fujitasz@kuee.kyoto-u.ac.jp; oda@flosfia.com

Received August 2, 2016; accepted September 9, 2016; published online November 17, 2016

The recent progress and development of corundum-structured III-oxide semiconductors are reviewed. They allow bandgap engineering from 3.7 to ~9 eV and function engineering, leading to highly durable electronic devices and deep ultraviolet optical devices as well as multifunctional devices. Mist chemical vapor deposition can be a simple and safe growth technology and is advantageous for reducing energy and cost for the growth. This is favorable for the wide commercial use of devices at low cost. The III-oxide semiconductors are promising candidates for new devices contributing to sustainable social, economic, and technological development for the future. © 2016 The Japan Society of Applied Physics

1. Introduction

The successful and dramatic evolution of wide-bandgap (WBG) semiconductors^{1–3)} represented by silicon carbide (SiC) and gallium nitride (GaN) is now followed by worldwide efforts to explore a new generation of materials, that is, ultra-wide-bandgap (UWBG) materials with bandgaps wider than those of SiC and GaN (>3.4 eV).⁴⁾ Examples of UWBG materials include aluminum nitride (AlN), aluminum gallium nitride (AlGaN), diamond, boron nitride (BN), and gallium oxide (Ga₂O₃).

Ga₂O₃ takes five different phases (α , β , γ , ϵ , and δ) and among them, the orthorhombic β -gallia structure (β -Ga₂O₃) is thermodynamically the most stable phase.^{5,6)} This has allowed the growth of single-crystalline β -Ga₂O₃ bulks, which are readily available as substrates, by conventional solution-based technologies such as floating-zone (FZ),^{7–9)} edge-defined film-fed growth (EFG),¹⁰⁾ Czochralski (CZ),^{11,12)} and vertical Bridgman (VB)¹³⁾ methods. This has been followed by successful homoepitaxy and doping of β -Ga₂O₃ layers^{14–20)} as well as marked development of β -Ga₂O₃-based Schottky barrier diodes (SBDs)^{17,21)} and transistors.^{17,18,22,23)} On the other hand, rhombohedral corundum-structured Ga₂O₃ (α -Ga₂O₃) is thermodynamically a semistable phase and was synthesized at high pressures.^{24,25)} Nevertheless, we showed the growth of α -Ga₂O₃ thin films on sapphire (α -Al₂O₃) substrates under atmospheric pressure at <500 °C.²⁶⁾

Indium oxide (In₂O₃) is also a III-oxide semiconductor and its stable phase is bixbyite.²⁷⁾ The growth of rhombohedral corundum-structured In₂O₃ (α -In₂O₃) had needed extremely high temperatures and high pressures,^{28–30)} but later α -In₂O₃ nanocubes³¹⁾ and nanorods³²⁾ were realized at ambient pressure. There have been a few reports on the growth of α -In₂O₃ thin films, but the films had poor crystallinity as highlighted by the full width at half maximum (FWHM) of X-ray diffraction (XRD) rocking curves for the (0006) diffraction of as broad as 1200 arcsec.³³⁾ Later, using an α -Fe₂O₃ buffer layer on a sapphire substrate the growth of α -In₂O₃ thin films with the (0006) XRD rocking curve FWHM of 182 arcsec was demonstrated.³⁴⁾

A series of studies achieving α -Ga₂O₃ and α -In₂O₃ encouraged the development of bandgap engineering with an alloy system consisting of α -Al₂O₃, α -Ga₂O₃, and α -In₂O₃. The density, a -axis length, c -axis length, ionic radii, and

Table I. Basic physical parameters of α -Al₂O₃, α -Ga₂O₃, and α -In₂O₃.

Crystal	Density (g/cm ³)	a -axis length (Å)	c -axis length (Å)	Ionic radii (Å)	Optical bandgap (eV)
α -Al ₂ O ₃	3.9956	4.754	12.99	0.535	8.75
α -Ga ₂ O ₃	6.4666	4.9825	13.433	0.62	5.3
α -In ₂ O ₃	7.3115	5.487	14.51	0.8	3.7

optical bandgap of α -Al₂O₃,^{35–37)} α -Ga₂O₃,^{24,26,37)} and α -In₂O₃.^{29,34,37)} are summarized in Table I. The relationships between bandgaps and average bond lengths are shown in Fig. 1, where those of β -Ga₂O₃ and several (U)WBG semiconductors are simultaneously displayed. In this alloy system, we can expect that bandgap energy is tuned between 3.7 eV (that of α -In₂O₃) and ~9 eV (that of α -Al₂O₃), keeping the corundum structure. In addition, a variety of heterostructures are expected under the conditions of lattice-matching or coherent growth. For β -Ga₂O₃, on the other hand, the bandgap energy was increased by partially substituting Ga with Al, that is, by forming β -(Al_{*x*}Ga_{1–*x*})₂O₃ alloys,^{38,39)} but the single β -phase was not maintained beyond the Al composition x of 0.61,³⁹⁾ because Al₂O₃ is stable in the α -phase. A similar phenomenon occurred for β -(In_{*x*}Ga_{1–*x*})₂O₃ alloys, with which the bandgap was reduced.⁴⁰⁾ Since the β -phase is characteristic to β -Ga₂O₃, the bandgap tuning is limited in the range near that of β -Ga₂O₃ and the crystallinity might be degraded in alloys owing to their immiscibility.

Corundum-structured III-oxide semiconductors based on α -Ga₂O₃ are promising for the wide design of heterostructure devices, and therefore research on their growth, properties, and devices is accelerating. In this paper, we briefly review the milestones in the evolution of this system from its dawn to the present day.

2. Growth of corundum III-oxides

2.1 Growth technologies

Corundum-structured α -Ga₂O₃ is mostly obtained on a sapphire (α -Al₂O₃) substrate, and this is probably due to the similarity in lattice structure between the epilayer and the substrate, despite the lattice mismatch (3.5 and 4.8% along the c - and a -axes, respectively). Interestingly for the growth, many of the studies on α -Ga₂O₃ have used mist chemical

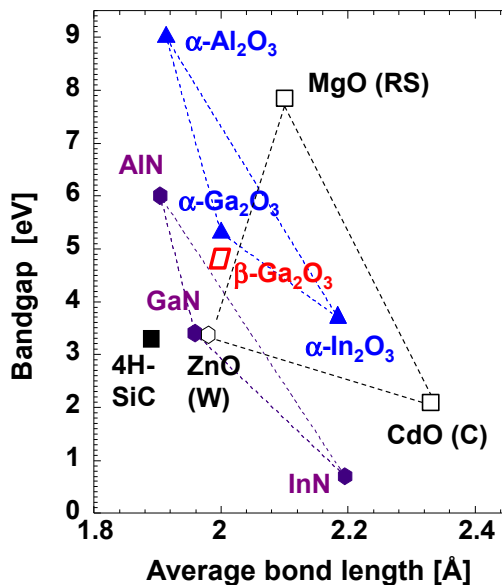


Fig. 1. (Color online) Relationships between bandgaps and average bond lengths of corundum-structured III-oxide semiconductors together with β - Ga_2O_3 and several (U)WBG semiconductors.

vapor deposition (CVD),^{24,41,42} whose details will be given in the following section, except for several works by molecular beam epitaxy (MBE)⁴³ and halide vapor phase epitaxy (HVPE).⁴⁴

It is natural that the crystal structure of the epilayer tends to follow that of the underlying layer and this has controlled the crystal structure of alloys constituted with binary compounds possessing different crystal structures, as discussed for ZnCdS ⁴⁵ and ZnMgO .⁴⁶ Nevertheless, many studies have shown the growth of β - Ga_2O_3 on sapphire by MBE,⁴⁷ pulsed laser deposition (PLD),⁴⁸ and metalorganic CVD (MOCVD).⁴⁹ One of the reasons for this discrepancy may be the difference in growth temperature, that is, the growth by MBE, PLD, and MOCVD has generally been carried out at high temperatures such as 700–800 °C in order to realize a more highly crystallized single phase. This naturally led to the growth of stable β - Ga_2O_3 . However, dominant β -phase was shown for Ga_2O_3 grown on sapphire by MBE even at 500 °C,⁴⁷ at which α - Ga_2O_3 is naturally grown by mist CVD. It is plausible that the low kinetic energy of precursors impinging onto the growth surface is one of the key factors for the grown films to follow the underlying crystal structure rather than to form a thermally stable phase.

For the growth of α - In_2O_3 on sapphire, the lattice mismatch is too large ($\sim 15\%$) to be overcome for the growth of a metastable phase. It has been reported that the use of α - Fe_2O_3 ³⁴ or α - Ga_2O_3 ⁵⁰ buffer layers, whose lattice constants are between those of α - In_2O_3 and sapphire, was effective for the growth of α - In_2O_3 on sapphire.

2.2 Mist CVD method

Mist CVD is a safe, cost-effective, and low-energy-consumption technology for the growth of oxide materials.^{51–56} An example of the growth system is shown in Fig. 2. In the growth of a metal oxide, water or alcohol solutions of safe and inexpensive chemicals containing the metal, for example, acetate or acetylacetonate, have been used as the source. By atomizing the source solution ultrasonically, it turns into mist

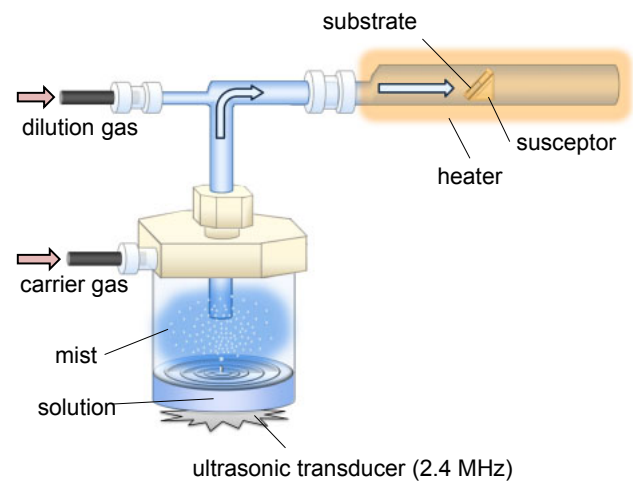


Fig. 2. (Color online) Example of mist CVD growth system for crystalline semiconductors.

particles (diameter of $\sim 3\ \mu\text{m}$ at an ultrasonic frequency of 2.4 MHz applied in our research), which are then transferred by a carrier gas to a reaction chamber. In this way, metal elements are supplied without the use of organometallic sources. They react with an oxygen source, which may be water, alcohol, or oxygen gas.

Mist CVD is effective in reducing the number of oxygen vacancies, which have been one of the serious issues in the growth of oxides. For example, room-temperature photoluminescence from ZnO layers grown by mist CVD is dominated by band-edge emission at $\sim 3.3\ \text{eV}$; we scarcely observed green emission at $\sim 2.3\ \text{eV}$, which is associated with oxygen vacancies, even when the ZnO layers were polycrystalline⁵⁷ or grown at low temperatures.⁵⁸ The growth is carried out under a sufficient supply of an oxygen source, that is, water or alcohol. This offers sufficient overpressure of oxygen with respect to the metal source and prevents the formation of oxygen vacancies.

3. Growth and properties of α - Ga_2O_3

3.1 Initial growth characteristics

Figure 3 shows the cross-sectional transmission electron microscopy (TEM) images at the α - Ga_2O_3 /sapphire interface observed along the $[11\bar{2}0]$ ⁵⁹ and $[10\bar{1}0]$ zone axes. In both images, it seems that the lattice mismatch is overcome within the several layers on the sapphire substrate, and defects are confined in these areas. Marked generation of dislocation lines penetrating into the α - Ga_2O_3 layer is hardly seen. Periodic structures were seen at the interface with the periods of 8.6 and 4.9 nm along $10\bar{1}0$ and $11\bar{2}0$, respectively. Since the lattice constants of α - Ga_2O_3 and sapphire are respectively 0.43 and 0.41 nm along $10\bar{1}0$, and 0.249 and 0.238 nm along $11\bar{2}0$, the periods of the structure coincide with 20 lattices of α - Ga_2O_3 and 21 lattices of α - Al_2O_3 both for $10\bar{1}0$ and $11\bar{2}0$. This suggests domain matching epitaxy⁶⁰ in the growth of α - Ga_2O_3 on sapphire.⁵⁹

Figure 4 shows the reciprocal space map for X-ray $10\bar{1}10$ diffraction of a thin (estimated to be 6 nm from the growth rate) α - Ga_2O_3 /sapphire sample. Peaks A and B correspond to diffractions from sapphire and α - Ga_2O_3 , respectively. It is worth noting that the reciprocal space coordinate (Q_x, Q_z) for peak B (α - Ga_2O_3) was almost the same as that

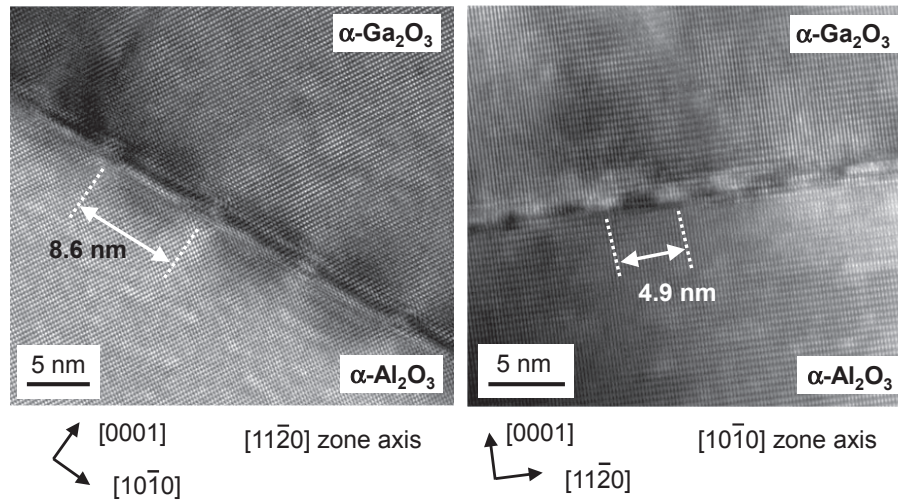


Fig. 3. Cross-sectional TEM images at α -Ga₂O₃/sapphire interface observed along [11 $\bar{2}$ 0]⁵⁹ and [10 $\bar{1}$ 0] zone axes.

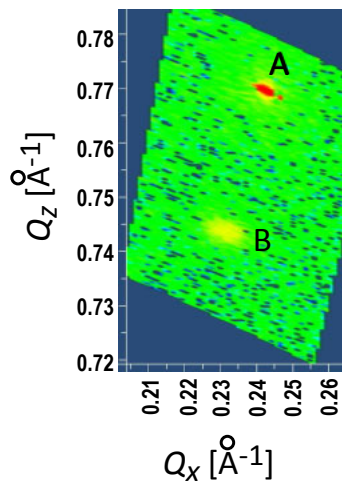


Fig. 4. (Color online) Reciprocal space map for X-ray 10 $\bar{1}$ 0 diffraction of thin (estimated to be 6 nm from the growth rate) α -Ga₂O₃/sapphire sample.

(0.232, 0.744) Å⁻¹ calculated from the lattice constants of strain-free α -Ga₂O₃ shown in Table I. This means that the lattice mismatch between α -Ga₂O₃ and sapphire is overcome at the very initial stage of the growth, supporting the TEM observation.

3.2 Structural properties

α -Ga₂O₃ on sapphire exhibits a very narrow spectrum in (0006) symmetric X-ray ω -scan diffraction. Typical FWHMs were as small as 30–60 arcsec. However, for antisymmetric (10 $\bar{1}$ 4) X-ray ω -scan diffraction, the FWHMs were as large as \sim 2000 arcsec for the α -Ga₂O₃ thicknesses of 300–2500 nm.

From the TEM observation shown in Fig. 3, the edge dislocation density was assessed as 7×10^{10} cm⁻² while the screw dislocation density was below the detection limit ($<10^7$ cm⁻²).⁵⁹ Because the lattice constant of α -Ga₂O₃ is larger than that of α -Al₂O₃, the α -Ga₂O₃ film is subjected to be in-plane compressive strain and strongly rocked by the α -Al₂O₃ crystal at the beginning of the growth. Therefore, it is necessary to introduce extra half-planes along { $\bar{2}$ 110} in the film to escape from the strain and successively grown. As a result, α -Ga₂O₃ thin films were grown as a semi-coherent

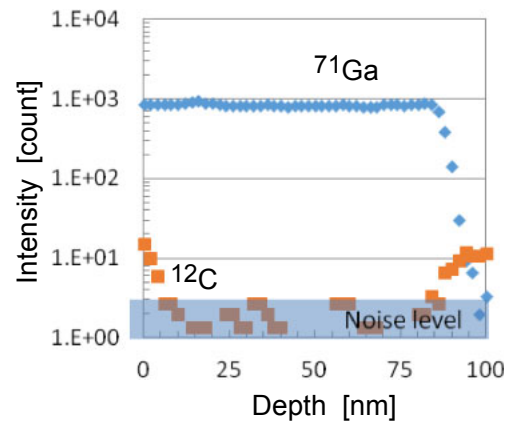


Fig. 5. (Color online) SIMS depth profiles of Ga and C.

mode.⁵⁹ The large FWHMs of XRD ω -scanning for anti-symmetric (10 $\bar{1}$ 4) and high density of edge dislocations can be explained by the introduction of the extra half-planes. The XRD profiles of antisymmetric planes contain information of crystal alignment of the out-of-planes and in-planes. Out-of-planes in α -Ga₂O₃ can easily keep parallel positions with respect to those in the substrate because α -Ga₂O₃ is rocked by the substrates. However, a disarray of crystals attributed to the existence of extra half-planes appears as an disorder of in-planes, resulting in huge FWHMs in in-plane XRD.

Impurities in α -Ga₂O₃ grown by mist CVD have been eliminated by careful modification of sources and growth equipment.⁶¹ Note that one can choose carbon-free sources, in mist CVD in contrast to MOCVD, such as gallium halides. With the use of these sources, carbon contamination level in the film was successfully decreased to be below the detection limit in secondary ion mass spectroscopy (SIMS), as shown in Fig. 5.

3.3 Electrical properties

Unintentionally doped (UID) α -Ga₂O₃ showed very high resistivity, but doping of Sn achieved n-type conductivity.^{41,62} At an early stage, it was difficult to control the carrier (electron) concentration in terms of Sn concentration, and the carrier concentration obtained was limited to 7×10^{18} (Ref. 41) or 2.7×10^{19} (Ref. 62) cm⁻³. Later, by improving

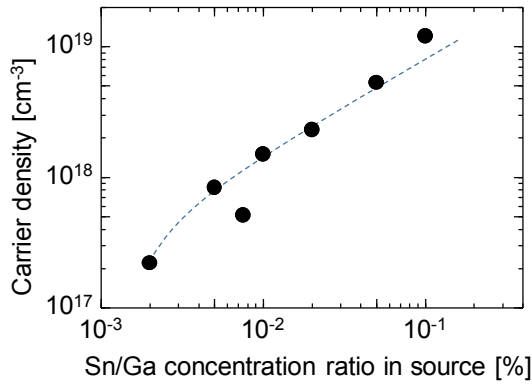


Fig. 6. (Color online) Carrier concentration in Sn-doped α -Ga₂O₃ against Sn source concentration in the source solution.⁶³⁾

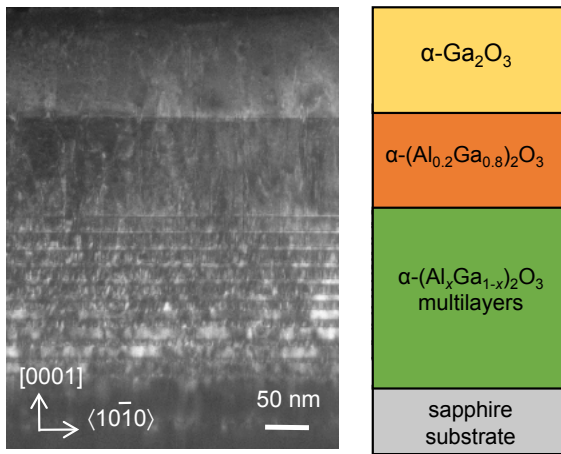


Fig. 7. (Color online) Cross-sectional TEM image at α -Ga₂O₃/sapphire interface with quasi-graded α -(Al_xGa_{1-x})₂O₃ buffer layers.⁶⁴⁾

the crystal quality, the carrier concentration was successfully controlled to be in the range of 10^{17} – 10^{19} cm⁻³ with respect to the Sn source concentration in the source solution, as shown in Fig. 6.⁶³⁾ Here, the thickness of the n-type α -Ga₂O₃ layer was 600 nm. However, the electron mobility was lower than 24 cm² V⁻¹ s⁻¹ and crystal defects such as dislocations severely restricted the mobility. Improvement of crystallinity is necessary for better electrical properties. On the other hand, the crystal quality becomes better with thickness and therefore in SBD structure, that is, n- on thick n+-layers, the n-type layer will have better electrical properties than the results shown above.

3.4 Buffer layers for defect control

In order to reduce the dislocation density in α -Ga₂O₃ layers, the use of strained buffer layers is reasonable. As an example, quasi-graded buffer layers, constituted of α -(Al_{0.9}Ga_{0.1})₂O₃/ α -(Al_{0.2}Ga_{0.8})₂O₃ multilayers, as shown in Fig. 7, were investigated.⁶⁴⁾ Here, by changing the thicknesses of the (Al_{0.9}Ga_{0.1})₂O₃ and (Al_{0.2}Ga_{0.8})₂O₃ layers, the average composition was gradually changed from (Al_{0.9}Ga_{0.1})₂O₃ to (Al_{0.2}Ga_{0.8})₂O₃. The TEM image shown in Fig. 7 demonstrates that dislocation defects tend to be confined in the buffer layers. The edge dislocation density was 6×10^8 cm⁻², which was two order of magnitude lower than that without buffer layers (7×10^{10} cm⁻², as shown above). However, screw dislocations were evident with a

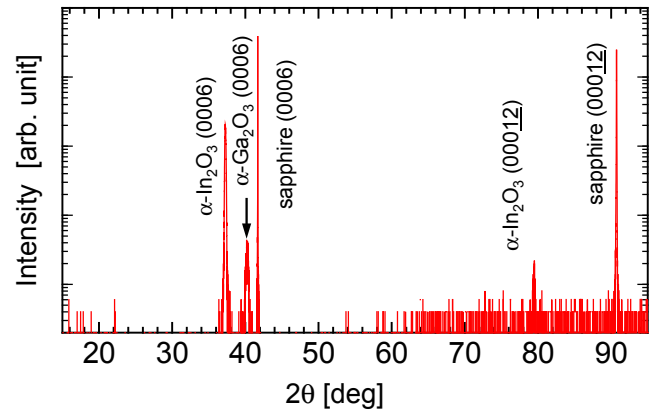


Fig. 8. (Color online) Example of $2\theta/\omega$ -scan XRD pattern of α -In₂O₃ grown on sapphire with α -Ga₂O₃ buffer layer.⁵⁰⁾

density of 3×10^8 cm⁻², which seemed to be due to the residual strain in the α -Ga₂O₃ layer as an effect of buffer layers. Further optimization of the buffer layer structures may lead to greater improvement of the quality.

3.5 Thermal stability

Since α -Ga₂O₃ takes a metastable phase, the inclusion of the β -phase was seen at growth temperatures higher than 550 °C²⁶⁾ and at successive annealing temperatures higher than 600 °C.⁶⁵⁾ This seriously limits the growth and process windows. However, it was found that slight (~1%) doping of Al markedly improved thermal stability. For example, single-phase α -Ga₂O₃:Al was grown at 550 °C and stable at 650 °C.⁶⁶⁾ Inclusion of more (~2.5%) inclusion of Al led to more stable films, that is, the α -phase was kept up to 750 °C, without marked widening of the bandgap. These phenomena may be similar to the solution hardening reported for GaAs doped with In,⁶⁷⁾ and can be applied as a useful technology to maintain the α -phase of Ga₂O₃ in the successive high temperature processes.

4. Growth and properties of α -In₂O₃

4.1 Buffer layers on sapphire substrates

The bandgap of α -In₂O₃ is 3.7 eV, which is reasonably high for power device applications. The electron effective mass in α -In₂O₃ is reported to be $0.16 m_0$,⁶⁸⁾ which is smaller than that of α -Ga₂O₃ ($0.276 m_0$).⁶⁹⁾ Here, m_0 denotes the electron mass in vacuum. Then, the mobility in α -In₂O₃ may be higher than that in α -Ga₂O₃, which is also an advantage for electron device applications.

However, the stable phase of In₂O₃ is bixbyite, and the lattice mismatch between α -In₂O₃ and sapphire, ~15%, is too large for α -In₂O₃ to take a corundum structure. Therefore, attempts have been made to use buffer layers for the growth of α -In₂O₃ on sapphire. As buffer layers, α -Fe₂O₃,³⁴⁾ α -Ga₂O₃,⁵⁰⁾ and α -(Al,Ga)₂O₃,⁷⁰⁾ whose lattice constants are between those of α -In₂O₃ and sapphire, are candidates.

4.2 Structural properties

With the use of buffer layers, single-phase corundum-structured α -In₂O₃ was successfully grown on sapphire. An example of a $2\theta/\omega$ -scan XRD pattern is shown in Fig. 8.⁵⁰⁾ The (0006) XRD ω -scan FWHM was, for example, 110 arcsec.

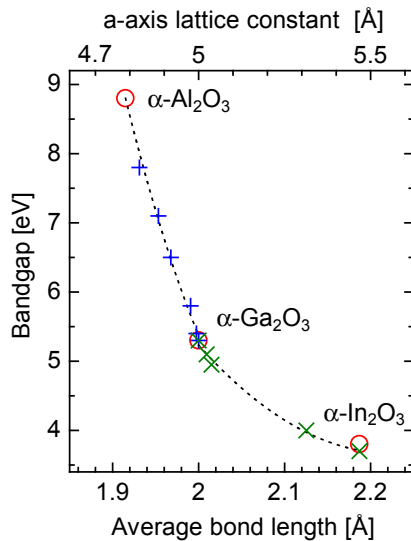


Fig. 9. (Color online) Bandgaps achieved by α -(Al,Ga) $_2$ O $_3$ and α -(In,Ga) $_2$ O $_3$ alloys.⁷¹⁾ The *a*-axis lattice constants are given in the sub-horizontal scale. Circles (red online) indicate the typical values for binary compounds.

4.3 Electrical properties

UID α -In $_2$ O $_3$ showed n-type conductivity with an electron concentration and a Hall mobility at room temperature of, for example, $3.1 \times 10^{18} \text{ cm}^{-3}$ and $143 \text{ cm}^2 \text{ V}^{-1} \text{ s}^{-1}$, respectively.⁷⁰⁾ The origin of donors is considered to be oxygen vacancies, speculated in analogy to other oxide semiconductors. As expected from the effective mass, the mobility is higher than that of α -Ga $_2$ O $_3$, suggesting the potential of α -In $_2$ O $_3$ for electrical device applications.

4.4 Thermal stability

Owing to the phase transition of α -Ga $_2$ O $_3$ to the β -phase occurring at the annealing temperature of 650 °C, as shown above, α -In $_2$ O $_3$ should be grown on an α -Ga $_2$ O $_3$ buffer layer below 650 °C. This was overcome by the use of α -(Al,Ga) $_2$ O $_3$ as a buffer layer, resulting in the growth of α -In $_2$ O $_3$ at temperatures as high as 850 °C.⁷⁰⁾ It can be concluded that α -In $_2$ O $_3$ is more thermally stable than α -Ga $_2$ O $_3$.

5. Growth and properties of corundum-structured III-oxide alloys

5.1 Bandgap engineering

The successful growth of α -Ga $_2$ O $_3$ and α -In $_2$ O $_3$ leads to bandgap engineering from 3.7 to ~ 9 eV by alloying α -Al $_2$ O $_3$, α -Ga $_2$ O $_3$, and α -In $_2$ O $_3$. Figure 9 shows the bandgaps achieved by α -(Al,Ga) $_2$ O $_3$ and α -(In,Ga) $_2$ O $_3$ alloys.⁷¹⁾ The bandgap can be tuned in almost the entire range except for 4.1–4.7 eV, where the phase separation of α -(In,Ga) $_2$ O $_3$ was recognized. Interestingly, this phenomenon is similar to that in InGaN.

The growth of alloys over a wide compositional range can be followed by the fabrication of heterostructures. Figure 10 illustrates the reciprocal space maps for X-ray 11 $\bar{2}$ 9 diffraction of α -(Al $_x$ Ga $_{1-x}$) $_2$ O $_3$ (thickness of ~ 100 nm) on α -Ga $_2$ O $_3$ for different compositions of *x*.⁷²⁾ On the basis of the lattice constant, α -Ga $_2$ O $_3$ was found to be completely lattice-relaxed. (Al $_x$ Ga $_{1-x}$) $_2$ O $_3$ layers, on the other hand, were coherently grown for *x* = 0.03 and 0.11, and that of *x* =

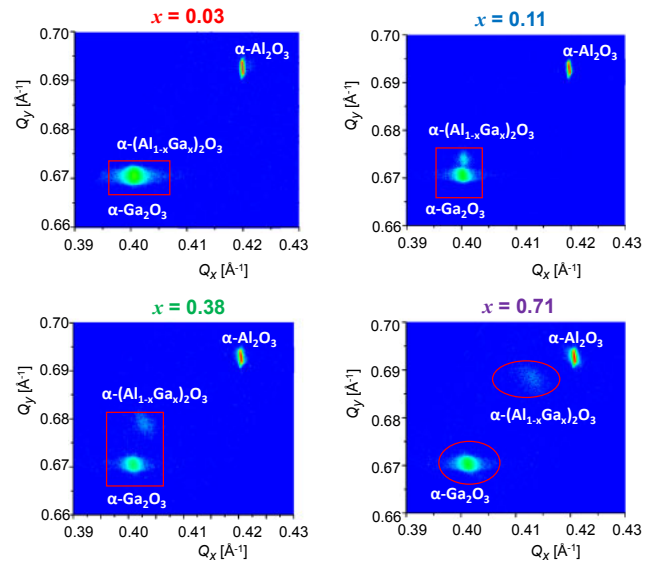


Fig. 10. (Color online) Reciprocal space maps for X-ray 11 $\bar{2}$ 9 diffraction of α -(Al $_x$ Ga $_{1-x}$) $_2$ O $_3$ (thickness of ~ 100 nm) on α -Ga $_2$ O $_3$ for different compositions of *x*.⁷²⁾

0.38 was slightly subjected to lattice relaxation. The sample of *x* = 0.71 was almost completely lattice-relaxed. According to the People–Bean model,⁷³⁾ the critical thicknesses were 2600, 210, 12, and 0.39 nm for *x* = 0.03, 0.11, 0.38, and 0.71. The results shown in Fig. 10 are totally explained by the People–Bean model.

Noted that uniform single-phase β -(Al $_x$ Ga $_{1-x}$) $_2$ O $_3$ is not grown for high Al compositions of *x*, because of the inclusion of the α -phase, which is the stable structure for Al $_2$ O $_3$.³⁹⁾ It is a crucial advantage that the entire compositional range can be covered by α -(Al $_x$ Ga $_{1-x}$) $_2$ O $_3$. X-ray photoemission spectroscopy (XPS) revealed that the β -(Al $_x$ Ga $_{1-x}$) $_2$ O $_3$ /Ga $_2$ O $_3$ heterostructure takes the type-I band lineup,⁷⁴⁾ which is favorable for applications to heterostructure transistors and multiple quantum wells.

5.2 Function engineering

There are a variety of corundum-structured transition-metal oxides such as α -Fe $_2$ O $_3$, α -Cr $_2$ O $_3$, and α -V $_2$ O $_3$, whose lattice constants (bond lengths) are within those of α -Al $_2$ O $_3$, α -Ga $_2$ O $_3$, and α -In $_2$ O $_3$. It is expected that alloying semiconductors with such oxides results in multifunctional properties on semiconductors. For example, above-room-temperature ferromagnetic properties together with semiconductor properties are demonstrated for α -(Ga,Fe) $_2$ O $_3$ ⁷⁵⁾ and α -(In,Fe) $_2$ O $_3$.⁷⁶⁾ This may lead to lattice-matched spintronic devices that are not severely affected by interface states between magnetic and semiconductor layers.

6. Devices with α -Ga $_2$ O $_3$

6.1 Potential of SBDs

Table II summarizes the expected performance of α -Ga $_2$ O $_3$ SBDs calculated from the well-known formula. Here, the breakdown field and relative permittivity were assumed to be 8 MV/cm and 10, respectively. Since the present controllable lower limit of donor concentration was estimated to be $1 \times 10^{17} \text{ cm}^{-3}$, the calculation was carried out for this condition as well as with the assumption of a donor ionization

Table II. Expected performance of α -Ga₂O₃ SBDs. Donor concentration was fixed at $1 \times 10^{17} \text{ cm}^{-3}$. For the on resistance of the n-layer, values were calculated assuming the mobility of 300 or 50 cm² V⁻¹ s⁻¹, and displayed in upper or lower lines, respectively.

Thickness of n-layer (μm)	Breakdown voltage (V)	On resistance (mΩ cm ²)	Donor concentration (cm ⁻³)
1	710	0.021 (300 cm ² V ⁻¹ s ⁻¹)	1×10^{17}
		0.125 (50 cm ² V ⁻¹ s ⁻¹)	
2	1238	0.042 (300 cm ² V ⁻¹ s ⁻¹)	1×10^{17}
		0.250 (50 cm ² V ⁻¹ s ⁻¹)	
3	1586	0.062 (300 cm ² V ⁻¹ s ⁻¹)	1×10^{17}
		0.375 (50 cm ² V ⁻¹ s ⁻¹)	
4	1752	0.083 (300 cm ² V ⁻¹ s ⁻¹)	1×10^{17}
		0.499 (50 cm ² V ⁻¹ s ⁻¹)	
5	1768	0.104 (300 cm ² V ⁻¹ s ⁻¹)	1×10^{17}
		0.624 (50 cm ² V ⁻¹ s ⁻¹)	

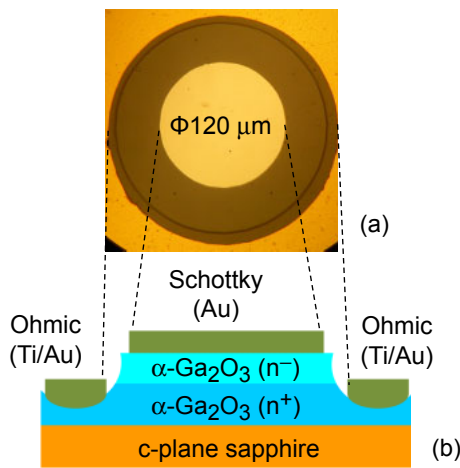


Fig. 11. (Color online) Schematic cross section of lateral-structure α -Ga₂O₃ SBDs.⁷⁷⁾

rate of 100%. As the mobility, 300 or 50 cm² V⁻¹ s⁻¹ was temporarily applied. Owing to the donor concentration, the breakdown voltage cannot be higher than 1800 V, but the devices with that of ~1000 V are within the target under the present technology.

6.2 Evolution of SBDs

Marked progress is going on for α -Ga₂O₃ SBDs at FLOSFIA, which are grown by mist CVD (MIST EPITAXY®). Because sapphire is an insulator, lateral structure SBDs as shown in Fig. 11 were investigated at the earliest stage.⁷⁷⁾ However, as shown later, the series resistance due to lateral current flow in the n⁺-layer was a serious problem. Then, an attempt was made to lift-off an α -Ga₂O₃ layer from sapphire, allowing the formation of vertical SBDs, as shown in Fig. 12.^{61,78)}

The forward current density versus voltage (J - V) characteristics of α -Ga₂O₃ SBDs are summarized in Fig. 13 for (a) a lateral SBD,⁷⁷⁾ (b) a vertical SBD (an initial device),⁷⁸⁾ and (c) vertical SBDs (advanced devices).⁶¹⁾ A marked increase of current density together with a reduction in on resistance was seen from (a) to (c). Table III summarizes the device structure and electrical properties of the SBDs. For the vertical SBDs, efforts had been made to improve the growth processes and device structures from the initial devices to the up-to-date devices. Among them, one of the keys was to

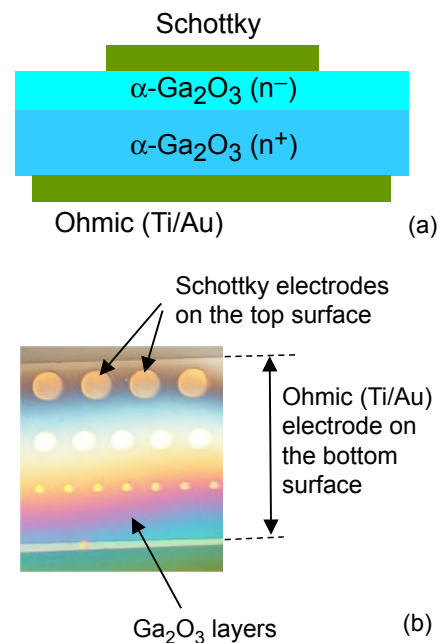


Fig. 12. (Color online) (a) Schematic cross section and (b) plain-view photograph of vertical-structure α -Ga₂O₃ SBDs.^{61,78)} In (b), note that the α -Ga₂O₃ layers are transparent in the visible region; the back ohmic contact is seen from the top.

change the Schottky contact metal from Au to Pt/Ti/Au, which reduces the built-in potential by more than 0.2 V.

Figure 14 compares the J - V characteristics of the four SBDs in a logarithmic plot of J . The lateral SBD (a) exhibited a large n value, suggesting large series resistance. It is worth noting that the vertical SBDs (b) and (c) showed nearly ideal n values (~1) but the linear regions in Fig. 14 are nearly parallel to each other with respect to the voltage. It is well known that the ideal relationship between J and V under thermionic emission theory is expressed as

$$J = A \cdot T^2 \cdot \exp\left(-\frac{q\phi_m}{k_B T}\right) \cdot \left[\exp\left(\frac{qV}{nk_B T}\right) - 1\right], \quad (1)$$

where ϕ_m , q , k_B , and T denote the Schottky barrier height, electronic charge, Boltzmann constant, and absolute temperature, respectively. A is a constant. When the ideality factors are the same, the parallel relationships in the plot between $\log J$ and V are attributable to the difference in $\exp(-q\phi_m/k_B T)$, that is, ϕ_m . If the reduction in built-in voltage,

Table III. Summary of SBD device properties.

Device	Configuration	Schottky contact	Built-in potential (eV)	n value	On resistance ($m\Omega cm^2$)	Breakdown voltage (V)
(a)	Lateral	Au		2.3		>500
(b)	Vertical	Au	1.7–2.0	1.1		270
(c) #1	Vertical	Pt/Ti/Au	~1.5	1.1	0.1	531
(c) #2	Vertical	Pt/Ti/Au	~1.5	1.1	0.4	855

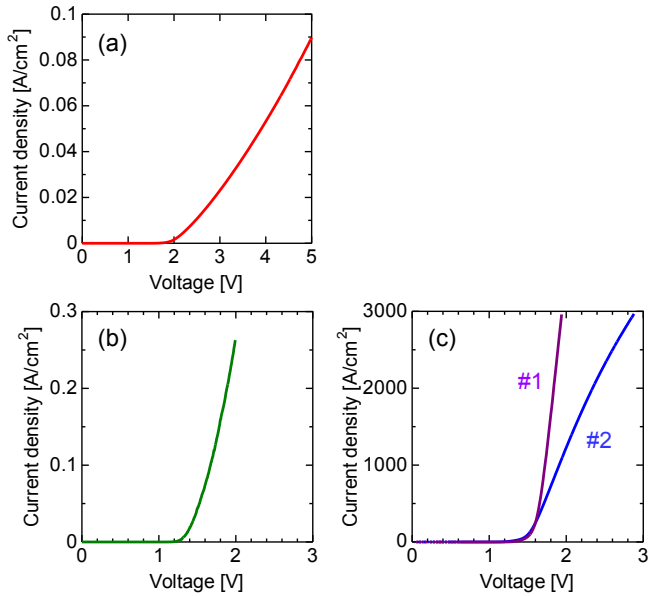


Fig. 13. (Color online) Forward J - V characteristics of α - Ga_2O_3 SBDs. (a) Lateral SBD,⁷⁷ (b) vertical SBD (initial device),⁷⁸ and (c) vertical SBDs (advanced devices).⁶¹

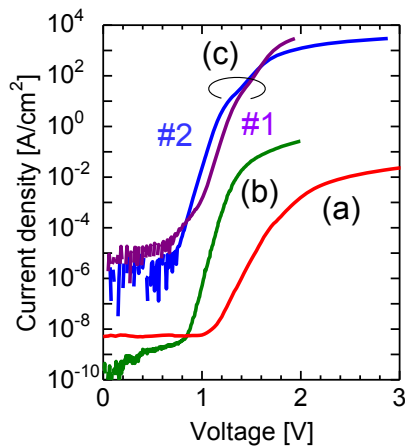


Fig. 14. (Color online) Comparison of forward J - V characteristics of a series of SBDs in logarithmic plot of J . (a) Lateral SBD,⁷⁷ (b) vertical SBD (initial device),⁷⁸ and (c) vertical SBDs (advanced devices).⁶¹

measured from capacitance–voltage measurements, by 0.2 eV is due to the reduction in ϕ_m by 0.2 eV, this results in an increase in J by more than three orders of magnitude.

A very low on resistance and high reverse breakdown voltage were apparently obtained. In the plot showing the relationship between the on resistance and the breakdown voltage, the data for the samples appeared close to or below the SiC limit. The use of mist CVD and sapphire substrates is

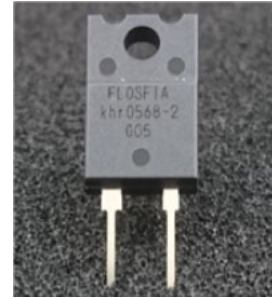


Fig. 15. (Color online) Photograph of the SBD in a TO package.

advantageous to reduce the device cost, leading to the supply of practical power devices to the market. Figure 15 is a photograph of the SBD in a transistor outline (TO) package.

6.3 Transistors

For transistors, on the other hand, metal–semiconductor field effect transistors (MESFETs) have been demonstrated.^{56,63} Their characteristics have not reached the standard of β - Ga_2O_3 , but we shall expect further evolution as well as the demonstration of high-performance MOSFETs.

7. Devices with α - In_2O_3

Owing to the mobility of higher than $100 cm^2 V^{-1} s^{-1}$ together with a wide bandgap of 3.7 eV, α - In_2O_3 can be considered as a candidate for electrical device applications. Preliminary MOSFETs have already been reported in the literature,⁵⁰ and efforts have been taken to improve their properties.

Since the electron concentration in UID α - In_2O_3 is $3.1 \times 10^{18} cm^{-3}$ or higher, it seems desirable to reduce it in order to fabricate MOSFETs with higher performance. This will be achieved in the future with the progress of growth technologies, but at the present stage the doping of Mg, which is expected to compensate for residual donors, was examined in a preliminary investigation. As a result, the carrier concentration was reduced to $1.2 \times 10^{18} cm^{-3}$ but the mobility was also reduced to $95 cm^2 V^{-1} s^{-1}$. However, the MOSFETs fabricated using amorphous Al_2O_3 as a gate insulator showed saturation and pinch-off behavior in drain characteristics and an on/off ratio of 10^5 in gate characteristics, as shown in Figs. 16(a) and 16(b), respectively.⁷⁰ The electrical properties were a subthreshold swing of 1.83 V/dec, a field-effect mobility of $187 cm^2 V^{-1} s^{-1}$, and an effective mobility of $240 cm^2 V^{-1} s^{-1}$. The relatively high mobilities are attractive for high-performance devices.

8. Summary and conclusions

In parallel to the recent progress of a variety of oxide semiconductors, corundum-structured III-oxide semiconduc-

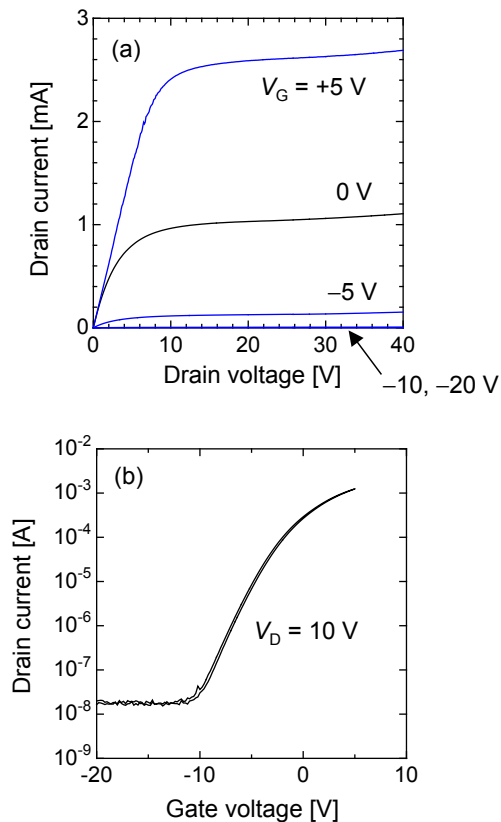


Fig. 16. (Color online) (a) Drain and (b) gate characteristics of α - In_2O_3 MOSFET.⁷⁰

tors offer opportunities for bandgap engineering in the (U)WBG region from 3.7 to ~ 9 eV and function engineering, leading to highly durable electronic devices and deep ultraviolet optical devices as well as multifunctional devices. The availability of simple and safe growth technologies such as mist CVD is also advantageous for reducing the energy and cost required for growth. We conclude that the recent marked progress in the fabrication of III-oxide semiconductors will be bloom for exploring sustainable social, economic, and technological development for the future.

Acknowledgments

The authors thank Dr. Kazuaki Akaiwa (presently at Tottori University), Takayuki Uchida, Masashi Kitajima, Riena Jinno, and Masashi Uchida for helpful support in experiments at Kyoto University as students. Appreciation is also due to Hitoshi Kanbara at FLOSFA Inc., for estimation of SBD device performance.

- 1) H. Amano, *Jpn. J. Appl. Phys.* **52**, 050001 (2013).
- 2) S. Fujita, *Jpn. J. Appl. Phys.* **54**, 030101 (2015).
- 3) T. Kimoto, *Jpn. J. Appl. Phys.* **54**, 040103 (2015).
- 4) R. J. Kaplar, A. A. Allerman, A. M. Armstrong, A. G. Baca, A. J. Fischer, J. J. Wierer, and J. C. Neely, *Abst. 228th Electrochemical Society Meet.*, 2015, MA2015-02, 1119.
- 5) R. Roy, V. G. Hill, and E. F. Osborn, *J. Am. Chem. Soc.* **74**, 719 (1952).
- 6) H. H. Tippins, *Phys. Rev.* **140**, A316 (1965).
- 7) N. Ueda, H. Hosono, R. Waseda, and H. Kawazoe, *Appl. Phys. Lett.* **70**, 3561 (1997).
- 8) E. G. Villora, K. Shimamura, Y. Yoshikawa, K. Aoki, and N. Ichinose, *J. Cryst. Growth* **270**, 420 (2004).
- 9) N. Suzuki, S. Ohira, M. Tanaka, T. Sugawara, K. Nakajima, and T. Shishido, *Phys. Status Solidi C* **4**, 2310 (2007).

- 10) H. Aida, K. Nishiguchi, H. Takeda, N. Aota, K. Sunakawa, and Y. Yaguchi, *Jpn. J. Appl. Phys.* **47**, 8506 (2008).
- 11) Y. Tomm, P. Reiche, D. Klimm, and T. Fukuda, *J. Cryst. Growth* **220**, 510 (2000).
- 12) Z. Galazka, R. Uecker, K. Irmischer, M. Albrecht, D. Klimm, M. Pietsch, M. Brützm, R. Bertram, S. Ganschow, and R. Fornari, *Cryst. Res. Technol.* **45**, 1229 (2010).
- 13) K. Hoshikawa, E. Ohba, T. Kobayashi, J. Yanagisawa, C. Miyagawa, and Y. Nakamura, *J. Cryst. Growth* **447**, 36 (2016).
- 14) E. G. Villora, K. Shimamura, K. Kitamura, and K. Aoki, *Appl. Phys. Lett.* **88**, 031105 (2006).
- 15) T. Oshima, N. Arai, N. Suzuki, S. Ohira, and S. Fujita, *Thin Solid Films* **516**, 5768 (2008).
- 16) K. Sasaki, A. Kuramata, T. Masui, E. G. Villora, K. Shimamura, and S. Yamakoshi, *Appl. Phys. Express* **5**, 035502 (2012).
- 17) K. Sasaki, M. Higashiwaki, A. Kuramata, T. Masui, and S. Yamakoshi, *J. Cryst. Growth* **378**, 591 (2013).
- 18) M. Higashiwaki, K. Sasaki, A. Kuramata, T. Masui, and S. Yamakoshi, *Phys. Status Solidi A* **211**, 21 (2014).
- 19) H. Okumura, M. Kita, K. Sasaki, A. Kuramata, M. Higashiwaki, and J. S. Speck, *Appl. Phys. Express* **7**, 095501 (2014).
- 20) H. Murakami, K. Nomura, K. Goto, K. Sasaki, K. Kawara, Q. T. Thieu, R. Togashi, Y. Kumagai, M. Higashiwaki, and A. Kuramata, *Appl. Phys. Express* **8**, 015503 (2015).
- 21) M. Higashiwaki, K. Konishi, K. Sasaki, K. Goto, K. Nomura, Q. T. Thieu, R. Togashi, H. Murakami, Y. Kumagai, B. Monemar, A. Koukitu, A. Kuramata, and S. Yamakoshi, *Appl. Phys. Lett.* **108**, 133503 (2016).
- 22) M. Higashiwaki, K. Sasaki, A. Kuramata, T. Masui, and S. Yamakoshi, *Appl. Phys. Lett.* **100**, 013504 (2012).
- 23) M. Higashiwaki, K. Sasaki, T. Kamimura, M. H. Wong, D. Krishnamurthy, A. Kuramata, T. Masui, and S. Yamakoshi, *Appl. Phys. Lett.* **103**, 123511 (2013).
- 24) M. Marezio and J. P. Remeika, *J. Chem. Phys.* **46**, 1862 (1967).
- 25) C. T. Prewitt, R. D. Shannon, D. B. Rogers, and A. W. Sleight, *Inorg. Chem.* **8**, 1985 (1969).
- 26) D. Shinohara and S. Fujita, *Jpn. J. Appl. Phys.* **47**, 7311 (2008).
- 27) A. Gurlo, P. Kroll, and R. Riedel, *Chem.—Eur. J.* **14**, 3306 (2008).
- 28) R. D. Shannon, *Solid State Commun.* **4**, 629 (1966).
- 29) C. T. Prewitt, R. D. Shannon, D. B. Rogers, and A. W. Sleight, *Inorg. Chem.* **8**, 1985 (1969).
- 30) T. Atou, K. Kusaba, K. Fukuoka, M. Kikuchi, and Y. Syono, *Solid State Chem.* **89**, 378 (1990).
- 31) C. H. Lee, M. Kim, T. Kim, A. Kim, J. Paek, J. W. Lee, S.-Y. Choi, K. Kim, J.-B. Park, and K. Lee, *J. Am. Chem. Soc.* **128**, 9326 (2006).
- 32) J. Q. Xu, Y. P. Chen, Q. Y. Pan, Q. Xiang, Z. X. Cheng, and X. W. Dong, *Nanotechnology* **18**, 115615 (2007).
- 33) Ch. Y. Wang, V. Cimall, H. Romanus, Th. Kups, G. Ecke, Th. Stauden, M. Ali, V. Lebedev, J. Pezoldt, and O. Ambacher, *Appl. Phys. Lett.* **89**, 011904 (2006).
- 34) N. Suzuki, K. Kaneko, and S. Fujita, *J. Cryst. Growth* **364**, 30 (2013).
- 35) M. E. Innocenzi, R. T. Swimm, M. Bass, R. H. French, A. B. Villaverde, and M. R. Kokta, *J. Appl. Phys.* **67**, 7542 (1990).
- 36) N. Ishizawa, T. Miyata, I. Minato, F. Marumo, and S. Iwai, *Acta Crystallogr., Sect. B* **36**, 228 (1980).
- 37) R. D. Shannon, *Acta Crystallogr., Sect. A* **32**, 751 (1976).
- 38) Y. Kokubun, K. Miura, F. Endo, and S. Nakagomi, *Appl. Phys. Lett.* **90**, 031912 (2007).
- 39) T. Oshima, T. Okuno, N. Arai, Y. Kobayashi, and S. Fujita, *Jpn. J. Appl. Phys.* **48**, 070202 (2009).
- 40) A. Kudo and I. Mikami, *J. Chem. Soc., Faraday Trans.* **94**, 2929 (1998).
- 41) T. Kawaharamura, G. T. Dang, and M. Furuta, *Jpn. J. Appl. Phys.* **51**, 040207 (2012).
- 42) R. Cuscó, N. Domènech-Amador, T. Hatakeyama, T. Yamaguchi, T. Honda, and L. Artús, *J. Appl. Phys.* **117**, 185706 (2015).
- 43) R. Kumaran, T. Tiedje, S. E. Webster, S. Penson, and W. Li, *Opt. Lett.* **35**, 3793 (2010).
- 44) Y. Oshima, E. G. Villora, and K. Shimamura, *Appl. Phys. Express* **8**, 055501 (2015).
- 45) S. Fujita, M. Funato, S. Hayashi, and Sg. Fujita, *Jpn. J. Appl. Phys.* **28**, L898 (1989).
- 46) T. Takagi, H. Tanaka, S. Fujita, and Sg. Fujita, *Jpn. J. Appl. Phys.* **42**, L401 (2003).
- 47) T. Oshima, T. Okuno, and S. Fujita, *Jpn. J. Appl. Phys.* **46**, 7217 (2007).
- 48) F. B. Zhang, K. Saito, T. Tanaka, M. Nishio, and Q. X. Guo, *J. Cryst. Growth* **387**, 96 (2014).
- 49) V. Gottschalch, K. Mergenthaler, G. Wagner, J. Bauer, H. Paetzelt, C. Sturm, and U. Teschne, *Phys. Status Solidi A* **206**, 243 (2009).

- 50) K. Kaneko, Y. Ito, T. Uchida, and S. Fujita, *Appl. Phys. Express* **8**, 095503 (2015).
- 51) T. Kawaharamura, H. Nishinaka, and S. Fujita, *Jpn. J. Appl. Phys.* **47**, 4669 (2008).
- 52) T. Kawaharamura and S. Fujita, *Phys. Status Solidi C* **5**, 3138 (2008).
- 53) H. Nishinaka, Y. Kamada, N. Kameyama, and S. Fujita, *Jpn. J. Appl. Phys.* **48**, 121103 (2009).
- 54) S. Fujita, K. Kaneko, T. Ikenoue, T. Kawaharamura, and M. Furuta, *Phys. Status Solidi C* **11**, 1225 (2014).
- 55) T. Kawaharamura, *Jpn. J. Appl. Phys.* **53**, 05FF08 (2014).
- 56) G. T. Dang, T. Kawaharamura, M. Furuta, and M. W. Allen, *IEEE Trans. Electron Devices* **62**, 3640 (2015).
- 57) T. Kawaharamura, H. Nishinaka, K. Kametani, Y. Masuda, M. Tanigaki, and S. Fujita, *Zairyo* **55**, 153 (2006) [in Japanese].
- 58) H. Nishinaka, T. Kawaharamura, and S. Fujita, *Jpn. J. Appl. Phys.* **46**, 6811 (2007).
- 59) K. Kaneko, H. Kawanowa, H. Ito, and S. Fujita, *Jpn. J. Appl. Phys.* **51**, 020201 (2012).
- 60) J. Narayan, *J. Appl. Phys.* **93**, 278 (2003).
- 61) M. Oda, R. Tokuda, H. Kambara, T. Tanikawa, T. Sasaki, and T. Hitora, *Appl. Phys. Express* **9**, 021101 (2016).
- 62) K. Akaiwa and S. Fujita, *Jpn. J. Appl. Phys.* **51**, 070203 (2012).
- 63) K. Akaiwa, K. Kaneko, K. Ichino, and S. Fujita, *Jpn. J. Appl. Phys.* **55**, 1202BA (2016).
- 64) R. Jinno, T. Uchida, K. Kaneko, and S. Fujita, *Appl. Phys. Express* **9**, 071101 (2016).
- 65) S.-D. Lee, K. Akaiwa, and S. Fujita, *Phys. Status Solidi C* **10**, 1592 (2013).
- 66) S.-D. Lee, Y. Ito, K. Kaneko, and S. Fujita, *Jpn. J. Appl. Phys.* **54**, 030301 (2015).
- 67) H. Ehrenreich and J. P. Hirth, *Appl. Phys. Lett.* **46**, 668 (1985).
- 68) F. Fuchs and F. Bechstedt, *Phys. Rev. B* **77**, 155107 (2008).
- 69) H. He, R. Orlando, M. A. Blanco, R. Pandey, E. Amzallag, I. Baraille, and M. Rérat, *Phys. Rev. B* **74**, 195123 (2006).
- 70) M. Kitajima, M. Eng. Thesis, Kyoto University (2016).
- 71) S. Fujita and K. Kaneko, *J. Cryst. Growth* **401**, 588 (2014).
- 72) K. Kaneko, K. Suzuki, Y. Ito, and S. Fujita, *J. Cryst. Growth* **436**, 150 (2016).
- 73) R. People and J. C. Bean, *Appl. Phys. Lett.* **47**, 322 (1985).
- 74) T. Uchida, R. Jinno, S. Takemoto, K. Kaneko, and S. Fujita, presented at 43rd Int. Symp. Compound Semiconductors, 2016, ThC1-5.
- 75) K. Kaneko, I. Takeya, S. Komori, and S. Fujita, *J. Appl. Phys.* **113**, 233901 (2013).
- 76) K. Akaiwa, K. Kaneko, S. Fujita, E. Chikoidze, and Y. Dumont, *Appl. Phys. Lett.* **106**, 062405 (2015).
- 77) M. Oda, A. Takatsuka, T. Hitora, J. Kikawa, K. Kaneko, and S. Fujita, Ext. Abstr. Int. Conf. Solid State Devices and Materials, 2014, p. 1004.
- 78) M. Oda, J. Kikawa, A. Takatsuka, R. Tokuda, T. Sasaki, K. Kaneko, S. Fujita, and T. Hitora, *Conf. Dig. 73rd Device Research Conf.*, 2015, p. 137.



Shizuo Fujita was born in Osaka in 1955. He obtained BS and MS degrees from Kyoto University in 1978 and 1980, respectively. Then he continued his research on physics of silicon nitride films as a research associate in Kyoto University and obtained Ph.D. degree in 1990. Thereafter his research has been directed to property control of compound and alloy semiconductors including arsenic, II–VI, and nitride semiconductors. Now he is a professor at Kyoto University and is studying on oxide semiconductors. He is a collaborating member of the Science Council of Japan and a fellow of the Japan Society of Applied Physics.



Masaya Oda was born in Kyoto in 1986. He obtained BS and MS degrees from Kyoto University in 2009 and 2011, respectively. Now he is an Executive Director of FLOSFIA Inc.



Kentaro Kaneko was born in Osaka in 1984. He obtained BS, MS, and Ph.D. degrees in Engineering from Osaka Prefecture University in 2008, Kyoto University in 2010 and in 2013, respectively. Among these carriers, he was engaged in a research of functional oxides as a doctor course fellow (DC1) of the Japan Society for the Promotion of Science (JSPS), and alloying of functional materials as a Post-doctor fellow (PD) of JSPS. He has worked as an assistant professor at Kyoto University since 2014. He is a member of Japan Society of Applied Physics.



Toshimi Hitora was born in Nara in 1975. He obtained BS and MS degrees respectively from Kyoto University and Nara Advanced Institute of Science and Technology in 1998 and 2000. He established start-up companies of ALGAN Inc. and Roca Inc. (presently FLOSFIA Inc.) in 2005 and 2011, respectively, and now he is the chief executive officer (CEO) of FLOSFIA Inc.